p-Type Conduction Characteristics of Lithium-Doped ZnO Nanowires

JunSeok Lee, SeungNam Cha, JongMin Kim, HyeWon Nam, SangHyo Lee, WonBae Ko, Kang L. Wang, JeaGun Park, and JinPyo Hong**

Nanostructured electronic devices are expected to facilitate the continuing miniaturization of electronic devices and enable ultralow power device operation. In particular, 1D nanostructures such as nanowires (NW) and nanotubes have attracted great interest over the past decade because of their specific physical properties and their potential as building blocks for next-generation nanoelectronic devices.[1,2] Among various 1D materials, zinc oxide (ZnO), which has a direct and wide bandgap, is a promising candidate for light-emitting diodes, UV and gas sensors, transistor channels, and other devices that can utilize the unique vertical alignment characteristics and highly ordered single crystalline properties of NW structures.[3–6] However, because undoped ZnO NWs are intrinsically n-type, their use in practical devices has been hindered and much effort has been dedicated toward the development of p-type ZnO NWs. In particular, control and manipulation of the doping process is increasingly becoming a key approach for the realization of p-type ZnO NWs.

To realize p-type ZnO NWs, the initial dopant candidates tested included group V elements to substitute for O and group III elements to substitute for Zn, despite the large size mismatches in both cases. Recently, group I species such as Li and Na have been used to synthesize p-type ZnO NWs based on the expectation that these elements would function as shallow acceptors in ZnO host materials.[7–9] Li has the smallest ionic radius (0.76 Å) of group I species, which is very close to that of Zn (0.74 Å). Furthermore, several reports of excited centers observed using electron paramagnetic resonance spectroscopy have indicated that Li atoms can act as shallow acceptors in substantial forms of Zn sites (Li_{Zn}).[10,11] In addition, it is well-known that Li has specific advantages over other dopant elements, such as the ease with which it loses its valence electron and the preference of the Li atom for the cation site.[7]

In this study, we report the effective hydrothermal synthesis of vertically oriented p-type ZnO:Li NWs using an aqueous solution with lithium nitrate as a dopant source. We analyzed the structural and electrical properties of the various ZnO NWs extensively. Specially, we systematically analyzed the effects of the post-annealing process on hydrothermally as-grown ZnO:Li NWs to confirm stable p-type conduction in the ZnO:Li NWs.

High-resolution transmission electron microscopy (HR-TEM, JEOL JEM-2100F) observations of undoped ZnO, as-grown ZnO:Li, and annealed ZnO:Li NWs, together with selective area electron diffraction patterns (SAEDs) demonstrated the variety in crystal structures of the growth products and some of the effects of Li dopants in typical aqueous synthesis. As shown in **Figure 1**a, undoped ZnO had a typical (0001) ZnO NW wurtzite structure. In contrast, the HR-TEM image of as-grown ZnO:Li (inset, Figure 1b) revealed the presence of an unusual additional layer (1 to 1.5 nm in thickness) that formed on the axial surfaces of Zn-polar ZnO NWs in contrast to undoped ZnO NWs. We attributed this additional layer in as-grown ZnO:Li to the lithium nitrate chemical dopant. The SAED pattern in Figure 1b also shows an unusual lattice point with interstitial forms of lithium (Li_i) (inset, indicated by circle) in the disrupted crystal lattices. Therefore, we hypothesize that the Li_i in as-grown ZnO:Li may occupy the empty cages of the wurtzite structure at the octahedral (Li_i^O) site, but not at the tetrahedral interstitial (Li_i^T) site, because the formation energy of Li_i^O ($E_f = -2.09$ eV) is 0.62 eV lower than that of Li_i^T ($E_f = -1.47$ eV) in the nucleation process.[7] The inset of Figure 1c indicates an indented interfacial layer in annealed ZnO:Li NWs and no Li_i was observed in the SAED patterns after the post-annealing process. Thus, the post-annealing process appears to have caused the Li_i atoms to migrate into the crystal lattice due to thermal diffusion, resulting in perfect crystal periodicity within the crystal lattice.[12] To further characterize the samples, lattice constants of each sample were systematically determined from the X-ray diffraction (XRD) reciprocal mapping (Figure 1d, details in the Supporting Information). Undoped ZnO had a smaller *c*-axis lattice constant (5.21 Å, similar to the reference value of bulk ZnO),[13] than those of the other samples (as-grown ZnO:Li: 5.37 Å and annealed ZnO:Li: 5.25 Å). Initially, Li atoms in as-grown ZnO:Li NWs were likely interstitial dopants or defects and they may have been located inside the cages of the wurtzite structure, or at the octahedral sites, resulting in a reasonable increase in the *c*-axis lattice constant. However, after annealing, the magnitude of the *c*-axis lattice constant of annealed ZnO:Li NWs decreased from 5.37 Å to 5.25 Å, indicating the migration of Li

J. Lee, H. Nam, S. Lee, W. Ko, Prof. J. Hong
Department of Physics
Hanyang University
Seoul, 133-791, South Korea
E-mail: jphong@hanyang.ac.kr
Dr. S. Cha, Dr. J. Kim
Samsung Advanced Institute of Technology
Yongin-Si, 446-712, South Korea
E-mail: chasn@samsung.com
Prof. K. L. Wang
Department of Electrical Engineering
University of California
Los Angeles, CA 90095, USA
J. Park
Department of Electrical and Computer Engineering
Hanyang University
Seoul 133-791, Korea

DOI: 10.1002/adma.201101376

© 2011 WILEY-VCH Verlag GmbH & Co. KGaA, Weinheim

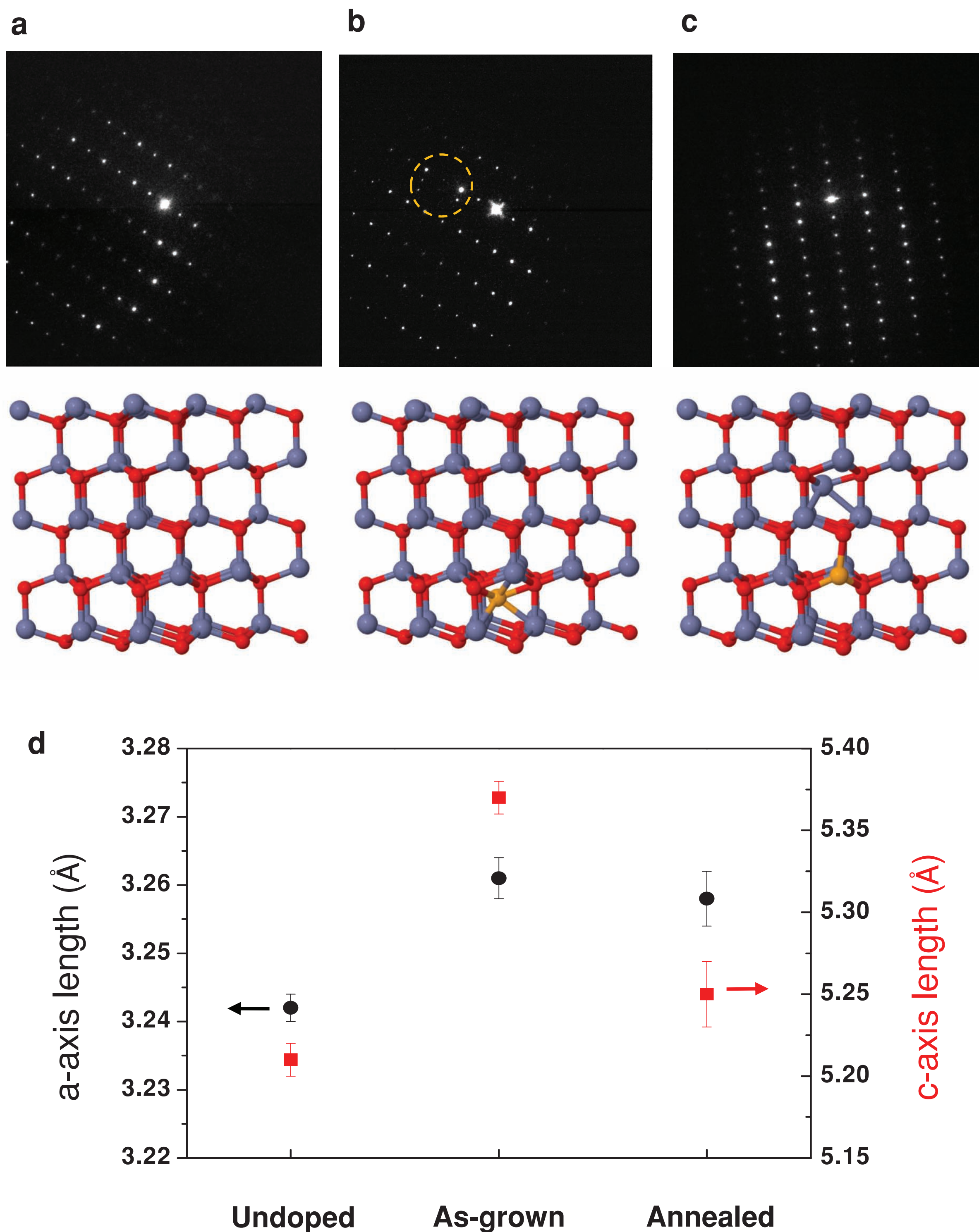

Figure 1. TEM measurements and structural configurations of each sample. a) Undoped ZnO NW with typical single crystal properties. b) The SAED pattern of the as-grown ZnO:Li NW had an unusual lattice point with an interstitial form of Li (Li_i^O, indicated by circle). c) Result of annealed ZnO:Li NW displayed an indented surface layer due to the post-annealing process. Bottom figures show simulations of possible structural geometries. d) The lattice constant was characterized by XRD analysis.

atoms due to annealing, followed by Li substitution of Zn. As a result, the lattice constant of annealed ZnO:Li NWs became slightly larger than that of undoped ZnO because the length of the Li–O bond (2.01 Å) is slightly larger than that of the Zn–O bond (1.97 Å). Therefore, after taking into account of the possible configuration geometries of three samples simulated by

© 2011 WILEY-VCH Verlag GmbH & Co. KGaA, Weinheim

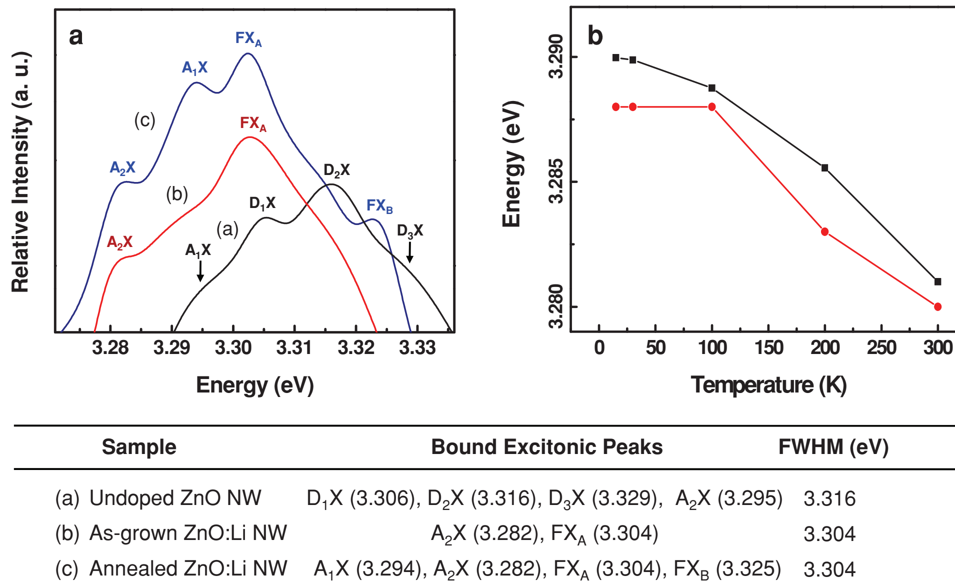

Sample	Bound Excitonic Peaks	FWHM (eV)
(a) Undoped ZnO NW	D_1X (3.306), D_2X (3.316), D_3X (3.329), A_2X (3.295)	3.316
(b) As-grown ZnO:Li NW	A_2X (3.282), FX_A (3.304)	3.304
(c) Annealed ZnO:Li NW	A_1X (3.294), A_2X (3.282), FX_A (3.304), FX_B (3.325)	3.304

Figure 2. Photoluminescence (PL) spectra of each sample at 10 K. a) Excitonic peaks of PL spectra of undoped ZnO (black line), as-grown ZnO:Li (red line), and annealed ZnO:Li NWs (blue line). Annealed ZnO:Li NWs provided fine free and acceptor-bound excitonic peaks. b) Temperature dependence of the transition energy of the excitonic peaks of annealed ZnO:Li NWs. The experimental results (black line) and theoretical values (red line) calculated using the Varshini equation.

the Perdew–Burke–Ernzerho theory with 45 unit cells,[7] we expect that when placed in the octahedral site, the Li atom in as-grown ZnO:Li is slightly displaced along the (0001) toward the neighboring oxygen atoms. While this interstitial Li atom in as-grown ZnO:Li has had little effect on the wurtzite structure, the *c*-axis lattice constant was increased. After the post-annealing process, the bottom image in Figure 1c indicated that the migration process between the interstitial Zn (Zn_i^O) atoms and the substitutional Li (Li_{Zn}) atoms led to a little decrease in the *c*-axis lattice constant, compared to that of as-grown ZnO:Li NWs.

Closer investigation of the fine structure of donor- and acceptor-bound excitonic emission peaks from the low-temperature photoluminescence (PL) spectra at 10 K provided significant insight into the effects of Li-doping and post-annealing (**Figure 2**a).[14] The PL spectrum of undoped ZnO NWs (black) clearly suggests n-type conduction with three donor-bound exciton peaks, in addition to a weak acceptor-bound exciton peak (A_2X). With Li-doping, these donor-bound exciton peaks disappeared, and the emergence of an acceptor-bound exciton peak (A_1X) and a free exciton peak (FX) implied a shift in the conduction behavior to p-type. Annealing the NWs after Li-doping resulted in further changes in the emission spectra and therefore the conduction type of the samples. The PL spectra of the annealed samples showed two free excitonic peaks (FX_A, FX_B) and two acceptor-bound exciton peaks (A_1X, A_2X). These results demonstrate that ZnO NWs of different conduction types can be synthesized by making simple changes to the growth process. The bottom table summarizes the bound exciton peaks and full width half-maximum (FWHM) for each sample. Figure 2b shows a plot of the experimental and theoretical values of free exciton emission energies for annealed ZnO:Li NWs as a function of temperature; the Varshini formula,

$$E_g(T) = E_g(0) - \alpha T^2/(T+\beta) \tag{1}$$

was used for theoretical evaluation. Here, $E_g(T)$ is the bandgap energy, T is the temperature (in K), and α and β are 1×10^{-4} eV and 700 K, respectively. Both theoretical and experimental results showed the same temperature-dependence trend.

In order to further infer doping-induced changes in the band structure and conduction type (i.e., p- or n- type) of a material from the PL characteristics, additional PL spectra of undoped ZnO, as-grown ZnO:Li, and annealed ZnO:Li NWs were collected at temperatures ranging from 10 K to 300 K (Figure S2, Supporting Information). In addition, the cathode luminescence (CL) spectra of annealed ZnO:Li NWs at room temperature were investigated to confirm the PL spectra results. Scanning electron microscopy (SEM), CL, and color mapping images of annealed ZnO:Li NWs show that clear, high-intensity emissions originated from annealed ZnO:Li NWs (Figure S3, Supporting Information).

To provide indirect evidence for the doping of Li after annealing, an electron energy loss spectroscopy (EELS) experiment using 200 kV scanning transmission electron microscopy (STEM) was performed (**Figure 3**). The signal peaks are plotted against electron energy loss, and the edge signals of the annealed ZnO:Li NWs (black), background (red), and spectrum (blue) are indicated. The EELS spectra of annealed ZnO:Li NWs clearly demonstrated Li K edge peaks at 62 eV, confirming the appearance of Li after annealing.

To confirm the p-type conduction of NWs, we fabricated a back gate NW field-effect transistor (NWFET) with a single annealed ZnO:Li NW as a p-channel. **Figure 4**a,b show typical source-to-drain current (I_{DS})–voltage (V_{DS}) p-type output at different gate voltages (V_G) and transfer characteristics from the device, where the measurement was performed in air at room

© 2011 WILEY-VCH Verlag GmbH & Co. KGaA, Weinheim

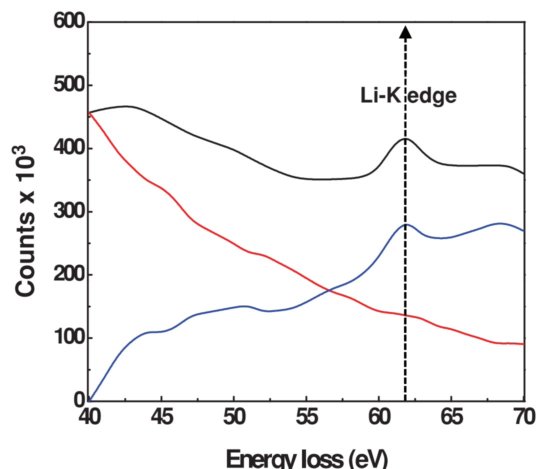

Figure 3. EELS spectrum of an annealed ZnO:Li NW. EELS spectrum of an annealed ZnO:Li NW with the background extrapolated using a log polynomial law fitting. The black line is the total signal, the red line is the background, and the blue line is the extracted ZnO NW signal. The extracted signal clearly showed a Li K edge peak at 62 eV.

temperature. The field-effect mobility of annealed ZnO:Li NWs is given by the following equation:

$$\mu_{FE} = (dI/dV_G)\ln(2h/r)/2\pi\varepsilon_0\varepsilon_r L/V_{DS} \quad (2)$$

where dI/dV_G is the transconductance (0.34 uS), ε_r is the dielectric constant of the SiO_2 gate oxide (3.9), ε_0 is the dielectric permittivity, h is the thickness of the gate oxide layer (300 nm), L is the channel length (500 nm), and r is the NW radius (80 nm).[15] Our NWFETs exhibited an carrier mobility of 2.52 $cm^2 V^{-1} s^{-1}$ and an effective hole carrier concentration of 1.68×10^{11} cm^{-3} is calculated from the equation

$$n = (V_G/e)(2\pi\varepsilon_0\varepsilon_r/\ln(2h/r)) \quad (3)$$

where e is the electron charge. The NWFET results demonstrate that the channel of annealed ZnO:Li NWs is p-type. Finally, to further confirm the stable p-type conductivity of the annealed ZnO:Li NWs, a simple n-type ZnO thin film (thickness 400 nm)/p-type post-annealed ZnO:Li NWs homojunction diode (length 1 μm) was prepared on a sapphire substrate. Al/Pt and Cr/Pt electrodes were used as n-type and p-type

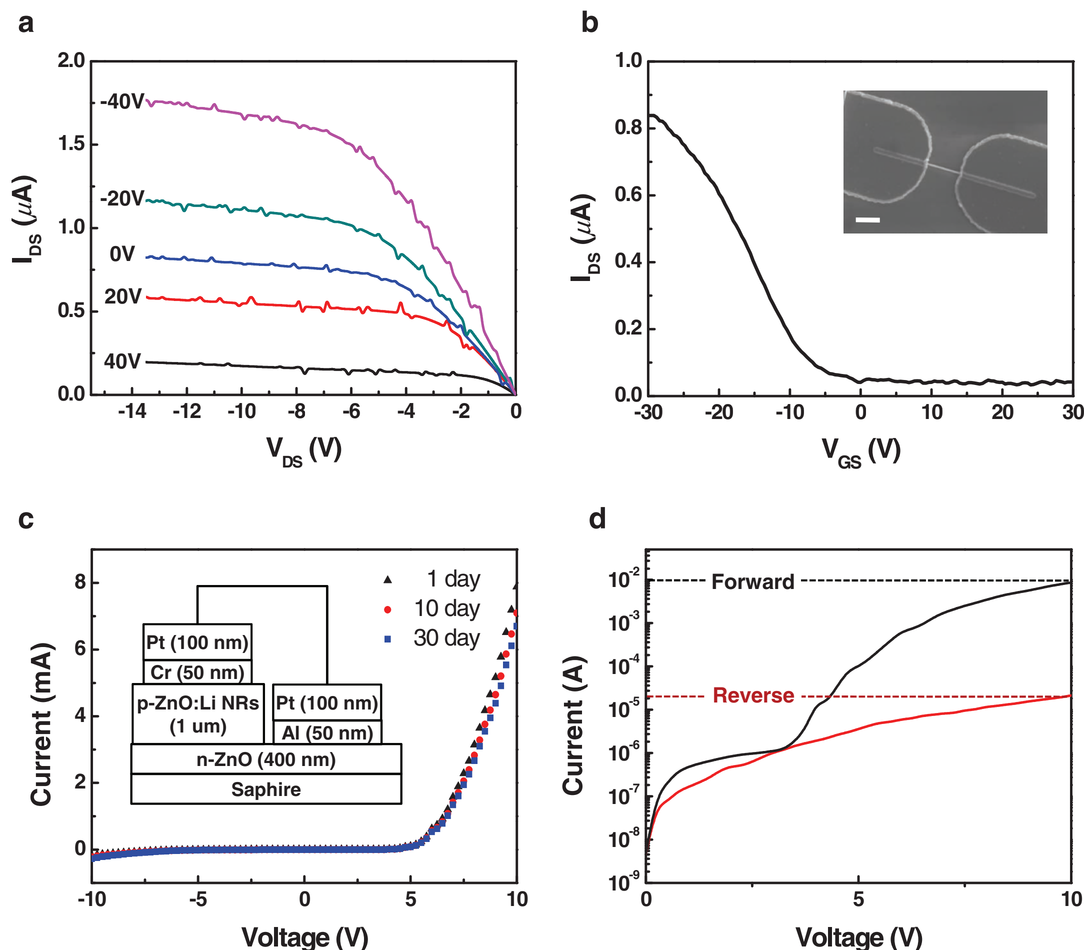

Figure 4. Electrical characteristics of a FET and p–n diode with an annealed ZnO:Li NW. a) Output properties of a back gate field-effect transistor with an annealed ZnO:Li nanowire. b) Transfer properties of annealed ZnO:Li NWFET at V_{DS} = 15 V. c) I–V behaviors of an n-type ZnO thin film/p-type ZnO:Li NW array diode. d) The semilogarithmic I–V plot for a typical p–n junction diode.

 © 2011 WILEY-VCH Verlag GmbH & Co. KGaA, Weinheim

contact layers, respectively. The current–voltage (I–V) measurements demonstrated typical rectification properties with a turn-on voltage of 5.5 V (Figure 4c). A plot of the logarithm of the current versus the voltage also exhibited a low reverse bias current at 10^{-5} A at a reverse bias of 10 V (Figure 4d).[16] As shown in Figure 4c,d, time-dependent measurements were performed for more than 30 days to confirm the stability of annealed ZnO:Li NWs. No significant variation in the p-type conduction of annealed ZnO:Li NWs was observed over time. However, even though our results conclusively demonstrate that Li can act as a p-type dopant in annealed ZnO:Li NWs after annealing, additional studies, including evaluation of different Li contents, various annealing processes, and diode devices, are required to further optimize the performance of our p-type ZnO NWs.

In summary, we described the growth of vertically aligned p-type ZnO:Li NWs based on a simple hydrothermal technique with a Li dopant in aqueous solution followed by post-annealing. TEM measurements of the *c*-axis oriented and highly vertically aligned NWs demonstrated that Li defects in as-grown ZnO:Li NWs can occupy the empty cages of the wurtzite structure at octahedral sites, and that Li substitution of Zn occurred because of thermally induced migration due to post-annealing in the presence of oxygen. We demonstrated the stable formation of p-type ZnO:Li NWs using a NW field-effect transistor and a simple n-type ZnO thin film/p-type annealed ZnO:Li NWs homojunction diode. Therefore, we expect that these simple synthesis concepts can be extended to other NW materials at low temperatures for potential applications in functional 1D oxide semiconductor devices.

Experimental Section

A-plane sapphire substrates were cleaned using a standard oxide wafer cleaning procedure. ZnO seed layers (10 nm-thick) were obtained from a ZnO ceramic target (99.95%, Kojundo) using an inductively coupled radio frequency (RF) plasma sputtering system to obtain a highly oriented columnar-grown seed layer (Figure S4, Supporting Information). The ZnO:Li NWs (1–2 µm long and up to 80 nm in diameter) were synthesized in an aqueous solution of 0.025 mmol aqueous zinc nitrate ($Zn(NO_3)_2 \cdot 6H_2O$, Sigma Aldrich), lithium nitrate ($Li(NO_3)$, Sigma Aldrich), and hexamethylenetetramine (HMT, Sigma Aldrich) in a digital water bath at a constant temperature of 92 °C. *A*-plane sapphire substrates with a deposited ZnO thin film were placed upside down in a quartz holder to avoid any metallic and self-assembly synthesized ZnO microcrystalline contamination. In addition, the hydrothermal syntheses were automatically processed on a precision pump drive systems (Masterflex) equipped with a digital mixer and a pH controller to accurately control the pH of the aqueous solutions. A continuous flow reactor was also developed to maintain a stable solution. The samples were then thoroughly washed with deionized water to eliminate residual salts. Finally, the post-annealing process was performed in O_2 gas at 500 °C to activate lithium dopants in as-grown ZnO NWs. Field-emission SEM (FE-SEM, Hitachi S-4800) and high-resolution XRD (HR-XRD, Bruker AXS D8) investigation of the ZnO:Li NWs deposited on a-plane sapphire substrates (2 in.) clearly demonstrated that the ZnO:Li NWs exhibited a *c*-axis oriented alignment structure (Figure S5, Supporting Information). The NWFET (inset, Figure 4b) was fabricated on a 300 nm thick SiO_2 gate oxide on n^+-Si wafer substrates using a KrF stepper and electron beam lithography (JEOL, JBX-9300FS). A Cr/Pt source, drain electrodes, and annealed ZnO:Li NW active channels were used for ohmic contact with p-type ZnO:Li active channel. Cr/Pt (20 nm/80 nm) and Al/Pt (80 nm/20 nm) electrodes were used for ohmic contact of a p-type ZnO:Li NW array and n-type ZnO thin film, respectively.

Supporting Information

Supporting Information is available from the Wiley Online Library or from the author.

Acknowledgements

The authors thank K. Kim, S. Jung of the Korea Advanced Nano Fab Center (KANC), and Dr. S. Kim of the Samsung Advanced Institute of Technology (SAIT) for experimental processes and helpful discussions with the manuscript. J.L. was supported by a grant from the Seoul Metropolitan Science Fellowship. This work was supported by a grant from the Korea Research Foundation funded by the Korean government (MOEHRD: 2010-0014680).

Received: April 12, 2011
Revised: July 3, 2011
Published online: August 11, 2011

[1] J. Xiang, W. Lu, Y. Hu, Y. Wu, H. Yan, C. M. Lieber, *Nature* **2006**, *441*, 489.
[2] A. M. Fennimore, T. D. Yuzvinsky, W-Qiang. Han, M. S. Fuhrer, J. Cumings, A. Zettl, *Nature* **2003**, *424*, 408.
[3] M. Sessolo, H. J. Bolink, *Adv. Mater.* **2006**, *6*, 1656.
[4] J. C. Johnson, K. P. Knutsen, H. Yan, M. Law, Y. Zhang, P. Yang, R. J. Saykally, *Nano Lett.* **2004**, *4*, 197.
[5] M. H. Huang, S. Mao, H. Feick, H. Yan, Y. Wu, H. Kind, E. Weber, R. Russo, P. Yang, *Science* **2001**, *292*, 1897.
[6] J. Goldberger, D. J. Sirbuly, M. D. Law, P. Yang, *J. Phys. Chem. B* **2005**, *109*, 9.
[7] A. Carvalho, A. Alkauskas, A. Pasquarello, A. K. Tagantsev, N. Setter, *Phys. Rev. B* **2009**, *80*, 195205.
[8] T. M. Børseth, F. Tuomisto, J. S. Christensen, W. Skorupa, E. V. Monakhov, B. G. Svensson, A. Y. Kuznetsov, *Phys. Rev. B* **2006**, *74*, 161202.
[9] V. Mauchamp, P. Moreau, G. Ouvrard, F. Boucher, *Phys. Rev. B* **2008**, *77*, 045117.
[10] Santa Chawla, K. Jayanthi, R. K. Kotnala, *Phys. Rev. B* **2009**, *79*, 125204.
[11] L. Wang, N. C. Giles, *J. Appl. Phys.* **2006**, *94*, 973.
[12] E. C. Lee, K. J. Chang, *Phys. Rev. B* **2004**, *70*, 115210.
[13] J. M. Recio, M. A. Blanco, V. Luaña, R. Pandey, L. Gerward, J. O. Staun, *Phys. Rev. B* **1998**, *58*, 8949.
[14] A. Teke, Ü. Özgür, S. Doğan, X. Gu, H. Morkoç, *Phys. Rev. B* **2004**, *70*, 195207.
[15] Y. C. Lee, Y. L. Chueh, C. H. Hsieh, M. T. Chang, L. J. Chou, Z. L. Wang, Y. W. Lan, C. D. Chen, H. Kurata, S. Isoda, *Small* **2007**, *3*, 1356.
[16] A. Tsukazaki, A. Ohtomo, T. Onuma, M. Ohtani, T. Makino, M. Sumiya, K. Ohtani, S. F. Chichibu, S. Fuke, Y. Segawa, H. Ohno, H. Koinuma, M. Kawasaki, *Nat. Mater.* **2005**, *4*, 42.

© 2011 WILEY-VCH Verlag GmbH & Co. KGaA, Weinheim